Acknowledgment

Partial funding for this work was sponsored by the Advanced Research Projects Agency (DoD) issued by U.S. Army Missile Command under Contract DAAH01-94-C-R278. The Raytheon authors thank H. Hendriks for polaron profiling, P. Lyman and J. Carter for MBE material growth, P. Jasion for SEM work, and D. Leveille for the PECVD of the SiN_x.

Manuscript submitted June 15, 1995; revised manuscript received Sept. 18, 1995. This was paper 772 presented at the Reno, NV, Meeting of the Society, May 21-26, 1995.

Raytheon Company assisted in meeting the publication costs of this article.

REFERENCES

1. T. Ono, M. Oda, C. Takahashi, and S. Matsuo, *J. Vac. Sci. Technol.*, **B4**, 696 (1986).
2. J. Asmussen, *ibid.*, **A7**, 883 (1989).
3. C. Constantine, D. Johnson, S. J. Pearton, U. K. Chakrabarti, A. B. Emerson, W. S. Hobson, and A. P. Kinsella, *ibid.*, **B8**, 596 (1990).
4. T. D. Mantei and T. E. Ryle, *ibid.*, **B9**, 29 (1991).
5. J. Hommel, F. Schneider, M. Moser, C. Geng, F. Scholz, and H. Schweizer, *Microelectron. Eng.*, **23**, 349 (1994).
6. S. Samukawa, *J. Vac. Sci. Technol.*, **B12**, 112 (1994).
7. P. K. Gadgil, T. D. Mantei, and X. C. Mu, *ibid.*, **B12** 102 (1994).
8. R. Cheung, Y. H. Lee, K. Y. Lee, T. P. Smith III, D. P. Kren, S. P. Beaumont, and C. D. W. Wilkinson, *ibid.*, **B7**, 1462 (1989).
9. T. Hara, J. Hiyoshi, H. Hamanaka, M. Sasaki, F. Kobayashi, K. Ukai, and T. Okada, *ibid.*, **67**, 2836 (1990).
10. K. K. Ko and S. W. Pang, *This Journal*, **141**, 255 (1994).
11. D. L. Flamm, V. M. Donnelly, and J. A. Mucha, *J. Appl. Phys.*, **52**, 3633 (1981).
12. R. N. Kackar and A. C. Shoemaker, *AT&T Technical J.*, **65**, 39 (1986).
13. G. E. P. Box, W. G. Hunter, and J. S.Hunter, *Statistics for Experiments*, John Wiley & Sons, New York (1978).
14. K. L. Seaward, N. J. Moll, and W. F. Stickle, *J. Electron. Mater.*, **19**, 385 (1990).
15. S. W. Pang, *This Journal*, **133**, 784 (1986).

A Reverse Monte Carlo Modeling Study of Diamond-like Carbon

J. S. Rigden* and R. J. Newport*

Physics Laboratory, The University of Kent at Canterbury, Canterbury, Kent CT2 7NR, England

ABSTRACT

Reverse Monte Carlo (RMC) modeling is a novel method of obtaining 3D information on atomic structure by combining complementary data from various experiments. X-ray and neutron diffraction data, nuclear magnetic resonance results, and chemical considerations have been used as constraints in the RMC process to model diamond-like carbon, an amorphous hydrogenated form of carbon with unusual properties. The results have given us new insight into this interesting material.

Introduction

In the last few years our knowledge of the properties of amorphous materials has grown considerably, and the number of their technological applications has multiplied. One such amorphous material, amorphous hydrogenated carbon (a-C:H), or diamond-like carbon, has been of particular interest due to its unusual physical and chemical properties. a-C:H can be made harder, denser, and more resistant to chemical attack than any other solid hydrocarbon and has a wide range of current and potential applications.[1]

Diamond-like carbon has been well characterized by the Kent Group, using various experimental techniques: neutron and x-ray diffraction, inelastic neutron scattering, and nuclear magnetic resonance (NMR).[2-4] These complementary results have provided a wealth of information on the structure and bonding environments within the material. Diffraction data, however, give an averaged representation of the structure and information on local arrangements is lost: to obtain a three-dimensional (3D) model of the structure of this important material, computer modeling techniques must be used. Reverse Monte Carlo (RMC) modeling is a method for producing a 3D representation of the structure of the material, which is consistent with both the experimental data to which it is fit, and any other constraints included in the model, *e.g.*, bonding considerations or chemical information.

* Electrochemical Society Active Member.

Theory

The validity of a structural model which is fit to experiment is clearly limited by the quality of the experimental data on which it is based. It is therefore extremely important to use high quality, carefully analyzed data. Full details of diffraction theory and the data analysis process can be found elsewhere, *e.g.*, Ref. 5, 6; the procedure is outlined only briefly herein.

An amorphous material can be described by its pair distribution function, $g(r)$, which is related to the number of atom centers at a distance r from a given atom at an arbitrary origin. The average number of atoms in a spherical shell of width dr, a distance r from an atom at the origin, is then given by

$$4\pi r^2 n_0 g(r) dr \qquad [1]$$

for an average number density n_0. For a multicomponent system with contributions from each pair type, a weighted combination of partial pair distribution functions is used.[7] According to the Faber-Ziman formalism[8] this is given by

$$G(r) = \sum c_\alpha b_\alpha c_\beta b_\beta g_{\alpha\beta}(r) \qquad [2]$$

where c_α is the atomic fraction of element α with scattering length b_α and $g_{\alpha\beta}(r)$ represents the partial terms in $G(r)$, *i.e.*, the number of β-type atoms about an α-type atom.

We can obtain a measure of the interference between scattering from neighboring atoms by Fourier transforming $G(r)$ to obtain the structure factor, $S(Q)$

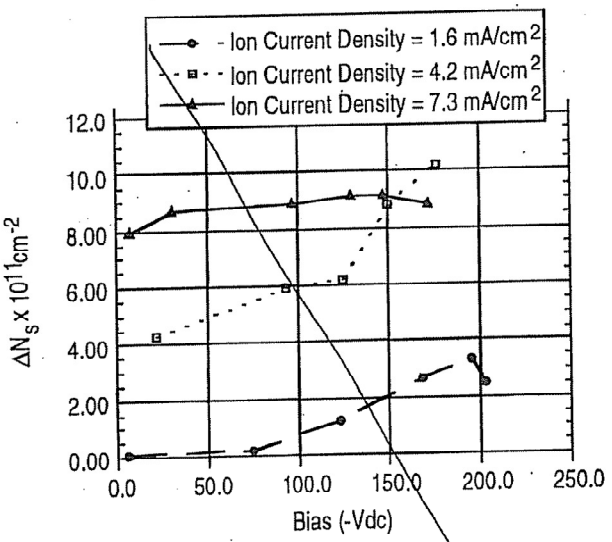

Fig. 5. Plot of ΔN_s vs. RF-induced dc bias as a function of ion current density. RF power was varied between 0 and 300 W. Damage test samples were exposed to the plasma for 60 s.

density and exposure time for times up to 120 s. With additional exposure to the plasma, the level of damage appears to saturate for all three values of ion current density. Saturation of damage has also been reported by others. Seaward *et al.*[14] observed a similar result for the RIE of SiO_2 on GaAs. Saturation of damage after extended exposure to the plasma was explained by a simple model of a layer devoid of carriers. In this model, carrier loss is caused by the introduction of deep acceptor levels into the GaAs layer. While this model may explain the dependence of damage on dose, it does not explain the damage dependence on ion current density observed here.

One possible hypothesis which explains the damage dependence on ion current density and the saturation of damage with exposure time is that a residual surface layer forms on the GaAs during plasma exposure. The nature of this surface layer is determined by the balance between ion and reactive neutral fluxes to the surface. In this picture, reactive neutrals lead to a buildup of either polymer (such as CF_x) or amorphous layers (such as GaF_x complexes) which buffer the underlying crystal substrate from the

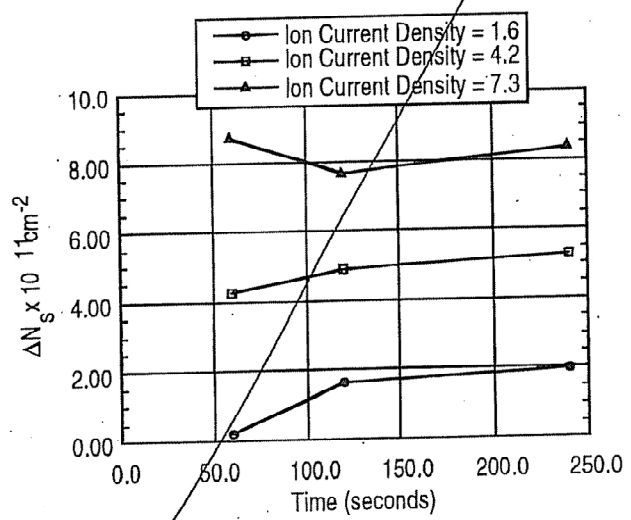

Fig. 6. ΔN_s vs. exposure time as a function of ion current density. Exposure time was varied from 60 to 240 s.

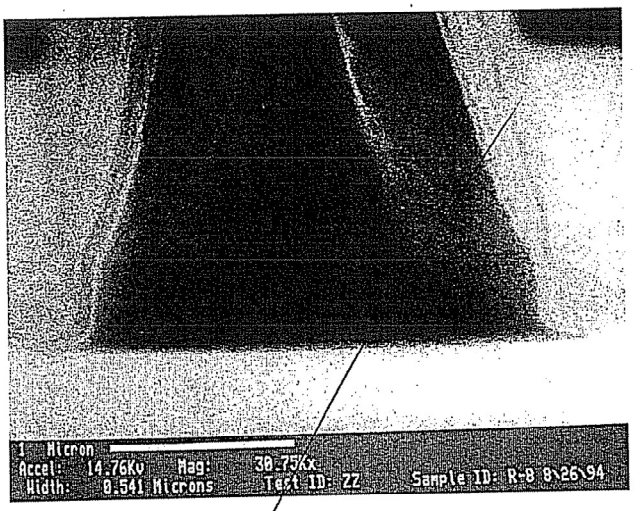

Fig. 7. SEM photograph of optimized sidewall.

incoming ion energy and prevent channeling. The thickness of this layer and the time for it to form is determined by the ratio of reactive neutrals which thickens the layer to ion flux which thins the layer by physical sputtering. For example, as the ion current density decreases, the ratio of ions to neutrals decreases, the surface layer thickness increases and protects the GaAs surface from the introduction of subsurface damage. This picture is consistent with the observations in RIE systems where the introduction of reactive gases was found to reduce the damage for a given RF bias when compared to an inert gas chemistry.[15] In this picture, the deep damage occurs primarily in the early plasma exposure before the surface layer was created while the crystal was open to channeling. Once the surface layer has formed the damage saturates (no additional damage is introduced for a given ion saturation current). Further experiments are needed to test this hypothesis and to determine the damage causing mechanisms which are relevant to this high ion current, low ion energy, low neutral pressure regime examined here.

A confirmation experiment was conducted to minimize ion current density and maximize RF power. Figure 7 shows an optimized sidewall of a sample etched at 500 W microwave power, 100 W RF power (−130 V_{dc}), 78 sccm total flow, 4 in. chuck height, 7% O_2, upper magnet current of 185 A, lower magnet current of 0 A, −5°C chuck temperature, and 10 mTorr chamber pressure. This optimized sample had a relatively low level of damage ($\Delta N_s = 0.77 \times 10^{11}$ cm^{-2}), ion current density of 1.6 mA/cm^2, selectivity of 1.4, uniformity of 2% across a 3 in. wafer, and an SiN_x etch rate of 78.4 nm/min.

Conclusion

Statistically designed experiments were performed to develop a high resolution etch process for the patterning of SiN_x layers over GaAs using a $CF_4/O_2/Ar$ plasma in an ECR. Plasma damage increased with increasing ion saturation current (first-order effect). Ion saturation current increased with decreasing chamber pressure. Damage was also increased with increasing ion energy, however this was a second-order effect. Damage saturated with exposure dose. Saturation of the damage may be explained by a residual surface layer forming on the GaAs during plasma exposure. The addition of low level RF power was necessary to provide profile control. A region in parameter space exists where low damage and anisotropy can be achieved simultaneously.

We have demonstrated that a high resolution, low damage $CF_4/O_2/Ar$ plasma etch process, for the patterning of submicron features in SiN_x films on GaAs substrates, was achieved in an ECR etch reactor.

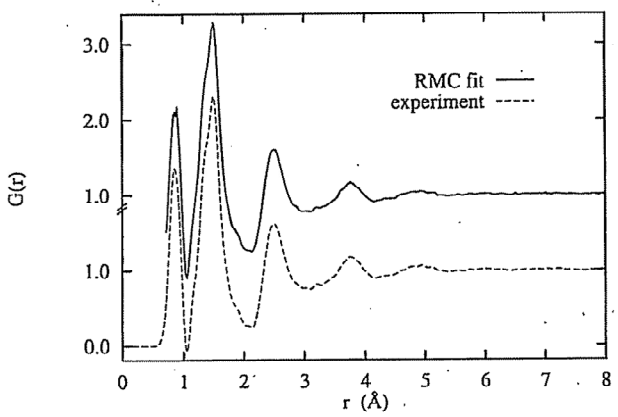

Fig. 2. Experimental $G(r)$ derived from neutron diffraction compared with the fit calculated from the RMC model.

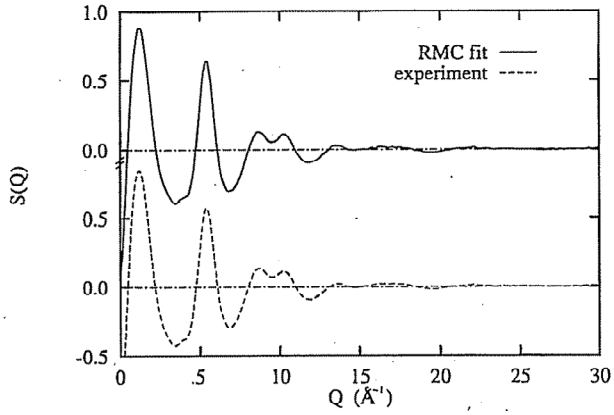

Fig. 4. Experimental $S(Q)$ obtained from neutron diffraction compared with the fit calculated from the RMC model.

This can be achieved in two ways: by using x-ray data where the contribution from the carbon dominates the diffraction pattern, or by limiting the neutron $G(r)$ to regions where only carbon-carbon correlations are present, for instance, the first C-C peak at ~1.4 Å. While the former case has the advantage that full $S(Q)$ data are used, and no additional errors are introduced into the data during the Fourier transform process to $G(r)$, the inherent difference in Q-space resolution between the neutron and x-ray data sets means that if a fit to the x-ray $S(Q)$ is obtained, then when neutron data is incorporated into the model, hydrogen atoms move into unphysical positions to compensate for the changed resolution. The latter option was used, therefore, to build the carbon matrix, and when a satisfactory fit was obtained to the first carbon coordination peak in the $G(r)$, the rest of the data set was included in the fit, along with the neutron $S(Q)$ data. The x-ray data sets may also be used in the fitting process, but must be included with low weightings; Fig. 1 shows the difference in resolution between the $G(r)$ for the neutron and x-ray data, and reveals the problems which result if the two data sets are used simultaneously with equal weighting. The x-ray data is therefore used as a broad constraint in the model by introducing a post-first shell constraint to the carbon network. This final model is allowed to run to equilibrium.

Results and Discussion

Figure 2 shows the experimental $G(r)$ obtained from the neutron diffraction data compared with that derived from the RMC model. The quality of the fit is evident; the RMC results are in good agreement with the data across most of the r-range. The first peak, however, at approximately 0.8 Å, is lower in the model than in experiment; this may be due to the higher uncertainty in the neutron diffraction data in this region due to strong inelastic scattering effects. The capacity of the RMC package to produce partial pair distribution functions means that it is possible to assign features of the distribution to specific bond types. Figure 3 shows the contributions to the $G(r)$ from each of the partial $g_{\alpha\beta}(r)$s (one for each pairing of atoms), calculated from the RMC fit. The strong negative scattering length for hydrogen means that correlations involving a single H atom have negative amplitude, whereas those with two or zero H atoms have positive amplitude. It is clear that the main shape of the pair distribution function above ~1 Å is due to carbon-carbon correlations, while the first peak at ~0.8 Å results from hydrogen-hydrogen correlations, *i.e.*, molecular hydrogen; this latter feature was also predicted by incoherent inelastic neutron scattering measurements.[3] It appears that $g_{CC}(r)$ falls abruptly at 1.25 Å, this value is defined in the RMC model to be the lower limit for the carbon-carbon interatomic distance, and is arguably too high. To compensate for this, hydrogen atoms have moved into positions in the model to fill this gap in the $G(r)$, which has resulted in an unphysical feature in $g_{HH}(r)$ in this region, and perhaps accounts for the unusual behavior of $g_{CH}(r)$ out to ~2 Å. This problem may be improved by exploring small iterations in the model cutoff values for the interatomic distances: in effect by varying the hard core radii within the model to offset the effects of instrumental resolution and the finite Q-range on the experimental $G(r)$, and hence on the model itself.

Figure 4 shows the experimental $S(Q)$ obtained from the neutron diffraction data, compared with the $S(Q)$ derived

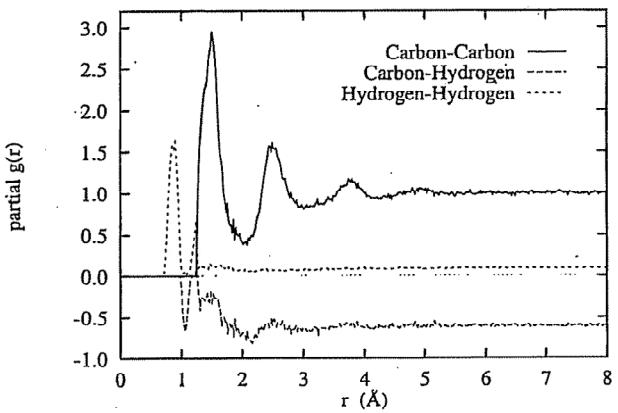

Fig. 3. Contributions to the RMC $G(r)$ from the partial $g(r)$ from each pair of atom types.

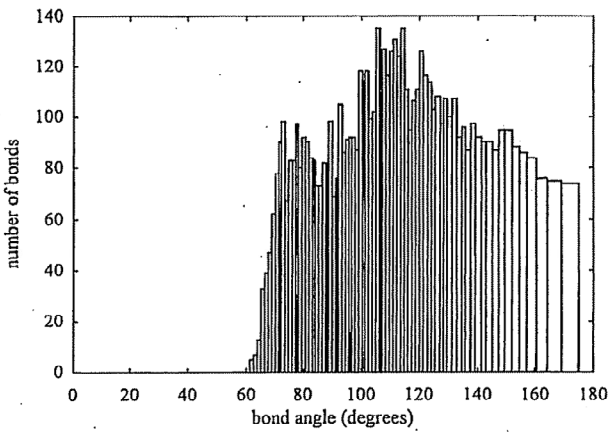

Fig. 5. The C-C-C bond angle distribution.

$$S(Q) = 1 + \frac{4\pi\rho}{Q}\int r[G(r) - 1]\sin(Qr)dr \qquad [3]$$

where $Q = 4\pi/\lambda \sin\theta$ is the momentum transfer on scattering through an angle 2θ, λ is the x-ray or (de Broglie) neutron wavelength, and ρ is the sample density; it is this structure factor which can be obtained directly from diffraction data. A similar set of formulae pertain to x-ray diffraction (XRD), although in this case the scattering length is modified by a form factor.

Experimental

The neutron diffraction measurements were undertaken using the liquid and amorphous diffractometer, LAD, at the pulsed neutron facility ISIS at the Rutherford Appleton Laboratory, UK, and the x-ray measurements on Station 9.1 at the Synchrotron Radiation Source at Daresbury Laboratory, UK; both instruments are detailed elsewhere.[5,9]

After suitable data reduction, *e.g.*, corrections for detector dead time, sample absorption, inelastic effects, etc., the structure factor, $S(Q)$, can be calculated

$$S(Q) = I_{eu}/N - f^2 \qquad [4]$$

where I_{eu} is the measured (corrected) scattered intensity (normalized to electron units in the case of XRD, N is the number of atoms in the sample, and f is the atomic form factor. (In practice, the scattered intensity is not measured in absolute units in the x-ray case, and the actual number of atoms, N, is not known: since f^2 is in electron units, the measured scattering can be scaled arbitrarily to oscillate about the f^2 term. For an amorphous material composed of more than one atom type, f^2 represents a weighted sum of the individual atomic form factors for each type.) This $S(Q)$ can be Fourier transformed in the appropriate manner to obtain the total pair distribution function, $G(r)$. Similar definitions are appropriate for neutron scattering and are detailed in Ref. 7.

The x-ray and neutron diffractometers produce data with different attributes. The x-ray data originating from Station 9.1 at the Daresbury Laboratory has a Q-range out to ~16.5Å^{-1}, with a high associated resolution, ~0.003 Å^{-1}. Despite the high Q-space resolution, the relatively short Q-range limits the resolution of the r-space $G(r)$ data ($\Delta r \sim 2\pi/Q_{max}$). The neutron diffractometer LAD at ISIS allows data to be collected out to $Q = 50$ Å^{-1}, with a resolution of 0.05 Å^{-1}; the neutron diffraction data therefore usually yields a higher resolution $G(r)$.

The scattering length b, in Eq. 2, gives a measure of the scattering power of each element for a particular radiation type. For x-rays, the scattering length for carbon is much higher than that of hydrogen, and hence XRD preferentially probes the carbon environment of the sample. Hydrogen has a large cross section for thermal neutron scattering, however, and hence neutron diffraction also reveals the hydrogen environment. The two techniques together therefore provide high quality, complementary information.

The RMC Technique

The basic RMC algorithm was conceived by McGreevy in 1988 and is detailed elsewhere.[10,11] In essence, the technique consists of moving atoms in a box until the derived pair distribution function and/or structure factor matches the experimental data:

1. A box is defined with side length at least twice the value of r at which significant oscillations in $G(r)$ disappear.
2. The box is randomly filled with atoms so that the number density of the box matches that of the material.
3. An atom is moved at random so that it does not overlap another.
4. The $G(r)$ and $S(Q)$, weighted for neutrons or x-rays are compared to the appropriate experimental data.
5. The discrepancy between the experiment and the fit is calculated. If the fit is improved the move is accepted; if the fit is not improved the move is rejected subject to a probability function dependent on the experimental error of the measurements.
6. Steps 1 to 3 are repeated until the model fit reproduces experiment to within experimental errors; where more than one data set is used, the acceptance/rejection criteria are applied to each.

RMC Model and Constraints

The initial box of atoms was constructed so as to mimic the sample conditions and to satisfy the above criteria. The initial configuration for a-C:H consisted of a random distribution of 5000 particles (3400 carbon atoms and 1600 hydrogen atoms, equivalent to the atomic proportions in the sample) at an atomic density of 0.14 atoms per Å^3, equivalent to the sample bulk density. The simulation was run on a DEC Alpha 3000 processor, where an average of ~10^6 moves may be attempted in a 24 h period. 10^7 attempted moves were required to fit the data and it was decided that the model had reached equilibrium when the ratio of moves tried to moves accepted had fallen to ~500:1.

The process of RMC modeling results in a configuration of atoms which is quantitatively consistent with the experimental data used to produce it. It is vital, however, to examine the produced model to assess whether it is a viable physical model. Previous experiments [2-4] have indicated that all atoms in a-C:H are bonded, that the bond angle distribution is centered around 109° (the tetrahedral angle) extending up to 120°, and that hydrogen atoms can bond to only one neighbor, carbon to no more than four neighbors. If the model produced by the RMC is not consistent with these constraints the model must be rejected, and the modeling process must be refined: this has been illustrated using the original RMC program with neutron diffraction data which resulted in an apparently good fit to the data. On more thorough analysis at the partial pair function level, however, it became clear that unphysical features were present in the configuration, *e.g.*, carbon atoms forming three-membered rings (triplets) or being bonded to more than four neighbors. The original code was modified to discourage the presence of triplets, and a constraint on the maximum number of neighbors was included.[12] The study was then continued using both neutron and XRD data, in both $S(Q)$ and $G(r)$ form.

Fitting Procedure

As well as introducing physical/chemical constraints into the RMC process to obtain a more realistic model, it is necessary to study the model as it progresses throughout the fitting procedure. In particular, for the case of a-C:H where the carbon atoms make up the main framework of the material, it is important to make sure that the skeleton of the network forms early on in the modeling process.

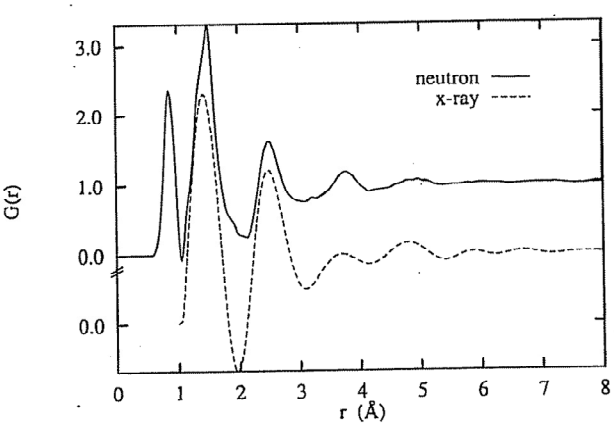

Fig. 1. Experimental $G(r)$ obtained from neutron and XRD; the difference in resolution is clear.

13. J. D. Wicks, Ph.D Thesis, Oxford University, Oxford, England (1993); D. W. Huxley, Private communication.
14. R. J. Newport, P. J. R. Honeybone, S. P. Cotterel, J. Franks, W. S. Howells, and R. J. Cernik, *Surf. Coatings Technol.*, **47**, 668 (1991).
15. D. W. Huxley, R. J. Newport, A. N. North, and J. K. Walters, *Mater. Res. Soc. Symp. Proc.*, **270**, 505 (1992).
16. J. S. Rigden, J. K. Walters, and R. J. Newport, *Phys. Scr.*, **T57**, 137 (1995).
17. M. A. Howe and R. L. McGreevy, Private communication.

Batch Reactor Kinetic Studies of Tungsten LPCVD from Silane and Tungsten Hexafluoride

David A. Bell,*[a] Carol M. McConica,* and Kevin L. Baker*

Department of Chemical and Bioresource Engineering, Colorado State University, Fort Collins, Colorado 80523, USA

Elizabeth Kuchta*

Institute of Physics, Technical University of Wroclaw, 50-370 Wroclaw, Poland

ABSTRACT

The silane (SiH_4) reduction of tungsten hexafluoride (WF_6), used to deposit tungsten during integrated circuit (IC) production, was investigated in a 0.64 liter, nonflowing laboratory reactor. Gas compositions were measured 2 mm from the growing surface, throughout time, with a mass spectrometer equipped with a capillary sampling tube. The initial partial pressures of SiH_4 and WF_6 ranged from 0.1 to 0.2 Torr. In each experiment, the kinetic rate dependence on concentration for a wide range of concentrations was observed as the reactants converted to products. Prior to heating the reactive surface, SiH_4 and WF_6 react at ambient temperature to produce gaseous $SiHF_3$ and SiF_4. The extent of this reaction can be suppressed by increasing the initial hydrogen partial pressure. On the 95°C surface, tungsten is deposited and $SiHF_3$ is the primary silicon fluoride reaction product for most of the tested conditions. A multiple regression analysis of 1,975 instantaneous composition/rate pairs gives orders of 1.22 in SiH_4, 0.27 in hydrogen, and −2.17 in WF_6. The order of dependencies on SiH_4 and WF_6 suggests that dissociative silane adsorption is the rate-limiting step and that WF_6 is the most abundant surface intermediate. The ratio of SiF_4 to $SiHF_3$ stays low and constant until the gas becomes very silane rich. Plots showing the evolution of the instantaneous rate over time imply that a minimal level of thermal activation of the reactive gas is necessary for the deposition to be surface rate limited.

Introduction

Chemical vapor deposition (CVD) is a commonly used technique for depositing thin films during the manufacturing of integrated circuits. Optimization of the deposition process is enhanced by a knowledge of the reaction kinetics. It has been the tradition in the IC industry to attempt to determine reaction kinetics from film thickness measurements taken at the end of a deposition in a flowing reactor which operates at steady state. The near-wafer gas composition is rarely measured. Most authors correlate inlet flow rates and total pressure to film thickness, without any knowledge of the true chemical composition driving film growth. An optimal set of flow rates in one reactor does not transfer to another reactor, because the hardware results in different reactant conversions and transport phenomena effects. Kinetic studies are best performed in a reactor where the instantaneous rate is determined from the dynamics of the chemical species and correlated with the actual chemical environment, as measured near the growing film. The instantaneous film growth rate can be determined from a mass balance on the instantaneous near-surface gas composition. The integrated film depth can be confirmed with postdeposition thickness measurements.

Tungsten is typically deposited by the reduction of gaseous tungsten hexafluoride (WF_6) with hydrogen (H_2) or silane (SiH_4). Published studies of SiH_4/WF_6 reaction kinetics present conflicting results. A review and analysis by Shon[1] showed that most of the published data were taken under mass-transfer limited conditions. Consequently, these are not valid kinetic studies. A notable exception is the recent paper by Ammerlaan *et al.*[2] They measured rates of weight gain for samples suspended from a microscale balance. For SiH_4/WF_6 pressure ratios less than 0.3, they found a 1.06 reaction order for SiH_4 and a −0.16 reaction order for WF_6. For SiH_4/WF_6 pressure ratios between 0.3 and 1.0, they found a 1.82 reaction order for SiH_4 and a −0.94 reaction order for WF_6.

The reaction pathway has also remained undefined since most deposition studies do not include observation of the chemical products. Silicon tetrafluoride (SiF_4) was long presumed to be a major reaction product of the SiH_4/WF_6 reaction

$$2WF_6(g) + 3SiH_4(g) \rightarrow 2W(s) + 3SiF_4(g) + 6H_2(g) \quad [1]$$

Other proposed reactions list hydrogen fluoride (HF) as a reaction product. Kobayashi *et al.*[3] used infrared spectroscopy to show that, under conditions of high partial pressures of WF_6, silicon hydrogen trifluoride ($SiHF_3$) is a major product and that SiF_4 is a minor product

$$WF_6(g) + 2SiH_4(g) \rightarrow W(s) + 2SiHF_3(g) + 3H_2(g) \quad [2]$$

Kobayashi *et al.*[3] noted that mass spectroscopy is the most common technique used to monitor CVD reactor gas-phase compositions and that the SiF^+_3 ion, which most investigators presumed to be a cracking fragment of SiF_4, is also a cracking fragment of $SiHF_3$.

Cheek *et al.*[4] have shown that either $SiHF_3$ or SiF_4 can be a major reaction product, depending upon the reaction conditions. They used a mass spectrometer equipped with a capillary sampling tube to measure near-surface concentrations of $SiHF_3$ and SiF_3 during deposition. The mass 67 ($SiHF^+_2$) to mass 85 (SiF^+_3) signal ratio declined with increasing SiH_4/WF_6 feed ratios up to a 1.3 feed ratio, and

* Electrochemical Society Active Member.
[a] Current address: Department of Chemical and Petroleum Engineering, University of Wyoming, Laramie, WY 82071-3295, USA.